

Molecular Mechanisms Underlying the Antitumor Activity of 3-Aminopropanamide Irreversible Inhibitors of the Epidermal Growth Factor Receptor in Non–Small Cell Lung Cancer^{1,2}

Elena Galvani^{*,†,3}, Elisa Giovannetti^{†,3}, Francesca Sacconi^{*}, Andrea Cavazzoni^{*}, Leticia G. Leon[‡], Henk Dekker[†], Roberta Alfieri^{*}, Caterina Carmi[§], Marco Mor[§], Andrea Ardizzoni[¶], Pier Giorgio Petronini^{*,3} and Godefridus J. Peters^{†,3}

^{*}Department of Clinical and Experimental Medicine, University of Parma, Parma, Italy; [†]Department Medical Oncology, VU University Medical Center, Amsterdam, The Netherlands; [‡]Biolab, Instituto Universitario de Bio-Orgánica Antonio Gonzalez, Universidad de La Laguna, Tenerife, Spain; [§]Pharmaceutical Department, University of Parma, Parma, Italy; [¶]Division of Medical Oncology, University Hospital of Parma, Parma, Italy

Abstract

Overcoming the emergence of acquired resistance to clinically approved epidermal growth factor receptor (EGFR) inhibitors is a major challenge in the treatment of advanced non–small cell lung cancer (NSCLC). The aim of this study was to investigate the effects of a series of novel compounds affecting viability of NSCLC NCI-H1975 cells (carrying the EGFR T790M mutation). The inhibition of the autophosphorylation of EGFR occurred at nanomolar concentrations and both UPR1282 and UPR1268 caused a significant induction of apoptosis. Targeting of EGFR and downstream pathways was confirmed by a peptide substrate array, which highlighted the inhibition of other kinases involved in NSCLC cell aggressive behavior. Accordingly, the drugs inhibited migration (about 30% vs. control), which could be, in part, explained also by the increase of E-cadherin expression. Additionally, we observed a contraction of the volume of H1975 spheroids, associated with the reduction of the cancer stem–like cell hallmark CD133. The activity of UPR1282 was retained in H1975 xenograft models where it determined tumor shrinkage ($P < .05$) and resulted well tolerated compared to canertinib. Of note, the kinase activity profile of UPR1282 on xenograft tumor tissues showed overlapping results with respect to the activity in H1975 cells, unraveling the inhibition of kinases involved in pivotal proliferation and invasive signaling pathways. In conclusion, UPR1282 and UPR1268 are effective against various processes involved in malignancy transformation and progression and may be promising compounds for the future treatment of gefitinib-resistant NSCLCs.

Neoplasia (2013) 15, 61–72

Abbreviations: CSCs, cancer stem cells; ECM, extracellular matrix; EGFR, epidermal growth factor receptor; EMT, epithelial-to-mesenchymal transition; FAK, focal adhesion kinase; NSCLC, non–small cell lung cancer; PCR, polymerase chain reaction; PDAC, pancreatic ductal adenocarcinoma; TKI, tyrosine kinase inhibitor
Address all correspondence to: Prof. Godefridus J. Peters, Department of Medical Oncology, VU University Medical Center, De Boelelaan 1117, 1081 HV Amsterdam, The Netherlands. E-mail: gj.peters@vumc.nl or Dott. Andrea Ardizzoni, Division of Medical Oncology, University Hospital of Parma, V.le Gramsci 14, 43126 Parma, Italy. E-mail: aardizzoni@ao.pr.it

¹This work was supported by Associazione Italiana per la Ricerca sul Cancro (AIRC), Milan grant IG 8856 (A.A.), the Netherlands Organization for Scientific Research (NWO), Veni grant; E. Giovannetti), AIRC-Marie Curie (International Fellowship; E. Giovannetti, and FIRC grant (Fellowship for abroad; E. Galvani).

²This article refers to supplementary material, which is designated by Figure W1 and is available online at www.neoplasia.com.

³These authors contributed equally to this study.

Revised 31 October 2012; Accepted 12 November 2012

Introduction

Non-small cell lung cancer (NSCLC) represents the majority of human epithelial cancers [1]. About 10% of NSCLCs is marked by functional activation of crucial “driver” oncoproteins with a pivotal dependency on growth factors and their receptors [2]. The epidermal growth factor receptor (EGFR) is a member of the ErbB family of receptor tyrosine kinases. These receptors are commonly expressed in different tissues of epithelial, mesenchymal, and neural origins and their pivotal role in normal individual development has been largely investigated. The involvement of EGFR in the regulation of important tumorigenic processes, such as proliferation, apoptosis, angiogenesis, and invasion, has also been demonstrated for different tumor types [3]. Furthermore, activated ErbB receptors stimulate several intracellular signaling pathways including the phosphatidylinositol 3-kinase/Akt/mammalian target of rapamycin and the Ras/Raf/mitogen-activated protein kinase pathways that have been demonstrated to play a key role in the control of numerous fundamental cellular processes. Along with its ligands (e.g., EGF, transforming growth factor- α , neuregulins), EGFR is often overexpressed and negatively correlated with prognosis in various tumor types, including NSCLC. In particular, the EGFR overexpression has been observed in 40% to 80% of NSCLC cases and multiple mutations of such receptor have been described and correlated with malignancy “oncogene addiction” [3]. Taken together, these findings identified EGFR as an ideal target for cancer therapy [4]. Small-molecule EGFR tyrosine kinase inhibitors (TKIs), such as gefitinib and erlotinib, have been approved as first-line treatment in selected NSCLC patients, as well as second/third-line treatment or maintenance therapy in unselected patients [3]. The clinical response to TKIs is correlated with activating EGFR mutations, predominantly the common in-frame deletions of exon 19 (delE746-A750) and the missense point mutation L858R. These aberrations are currently used as biomarkers to select patients more likely to benefit from EGFR TKIs as first-line treatment [5]. Unfortunately, after a progression-free period of about 10 months, most of the patients responsive to EGFR TKIs inevitably relapse. The acquired resistance to first-generation EGFR TKIs can be caused by multiple mechanisms, including the secondary EGFR point mutation T790M that accounts for ~50% of the cases [6,7]. The amplification of the receptor for the hepatocyte growth factor (c-Met) was also described as important mechanism of acquired resistance to gefitinib or erlotinib being observed in 20% of the cases [8]. The coexistence of the T790M mutation with c-Met amplification was rarely described [9].

A covalent interaction between EGFR TKIs with a cysteine residue located at the entrance of the EGFR adenosine triphosphate-binding cleft (Cys⁷⁹⁷) was described as a possible mechanism to bypass the T790M-related resistance to gefitinib. Several second-generation irreversible inhibitors have been developed [10–13], and many compounds, such as canertinib [14], afatinib [15], neratinib [16], and dacomitinib [17], progressed to clinical investigation, with mixed results. Therefore, acquired resistance against first-line EGFR inhibitors so far remains one of the major challenges for NSCLC treatment and the identification of new molecules targeting EGFR T790M mutants is warranted.

Furthermore, other factors might lay the foundation of drug resistance and novel compounds should be evaluated for their abilities to overcome also these emerging mechanisms. Recent studies reported the epithelial-to-mesenchymal transition (EMT) as a pivotal mechanism involved in the resistance of cancer cells against conventional therapeutics [18,19]. The EMT process results from a number of

dramatic cellular and molecular changes, including dissolution of adherent junctions, reorganization of the cytoskeleton, loss of cell polarity, induction of pro-mesenchymal gene expression, and migration through basement membranes and tissues. Several studies reported the reduction of the expression of the epithelial cell junction protein E-cadherin as key biomarker of EMT in the development of resistance to EGFR inhibition in lung cancer [20]. Importantly, the EMT is also involved in the acquisition of tumor stem-like cell phenotype characterized by high potential of self-renewal *in vitro* and tumorigenicity *in vivo* [21].

We recently developed a new series of irreversible EGFR inhibitors containing a 3-aminopropanamide fragment. The cytotoxicity of these compounds was previously tested *in vitro* in NSCLC H1975 cells [22]. Importantly, these molecules inhibited cell growth at considerably lower concentrations than gefitinib, showing irreversible inhibition of EGFR autophosphorylation, in spite of the lack of a cysteine-trapping warhead [22]. These compounds, while chemically stable in the extracellular environment, proved to be able to release an acrylamide derivative by retro-Michael degradation of the 3-aminopropanamide fragment in the intracellular environment. In principle, replacing the reactive acrylamide group of typical second-generation EGFR inhibitors by a chemically stable and basic aminopropanamide should confer both pharmaceutical (increased stability, water solubility, and bioavailability) and therapeutic (lower propensity to give nonspecific adducts with biological tissues) advantages. However, the ability of these pro-covalent inhibitors to exert antiproliferative activity on tumor cells can depend on the specific intracellular environment and must therefore be thoroughly examined. In particular, we investigated the activity of the 4-(3-chloro-4-fluoroanilino)-7-ethoxyquinazolino derivative UPR1282 and the 4-anilinoquinoline-3-carbonitrile derivative UPR1268 (Figure 1A) in both *in vitro* and *in vivo* models derived from the established gefitinib-resistant NSCLC H1975 cell line, which harbors the EGFR T790M mutation. Other pancreatic and lung cancer cell lines were included in this investigation to compare and understand their effects in diseases where EGFR inhibitors have demonstrated to be active.

Materials and Methods

Drugs and Chemicals

The synthesis of UPR1282 and UPR1268 has previously been described by Carmi et al. [22]. Gefitinib was a generous gift from AstraZeneca (Macclesfield, United Kingdom). The drugs were dissolved in DMSO at the stock concentration of 10 mM and then diluted for the experiments in culture medium before use. RPMI medium, FBS, penicillin (50 IU/ml), and streptomycin (50 μ g/ml) were from Gibco (Gaithersburg, MD). All other chemicals were purchased from Sigma-Aldrich (Zwijndrecht, The Netherlands).

Cell Culture

The human NSCLC cell lines NCI-H1975 (H1975), Calu-1, and A549 and the pancreatic ductal adenocarcinoma (PDAC) cell lines PANC-1 and MIA PaCa-2 were purchased from ATCC (Manassas, VA) and cultured as recommended. Cells were maintained as monolayers in RPMI 1640 (containing 2 mM L-glutamine) supplemented with 10% heat-inactivated FBS and 1% streptomycin and penicillin in a 37°C water-saturated atmosphere of 5% CO₂ in air in 75-cm² tissue culture flasks (Costar, Cambridge, MA). The cell lines were tested for their authentication by polymerase chain reaction (PCR)

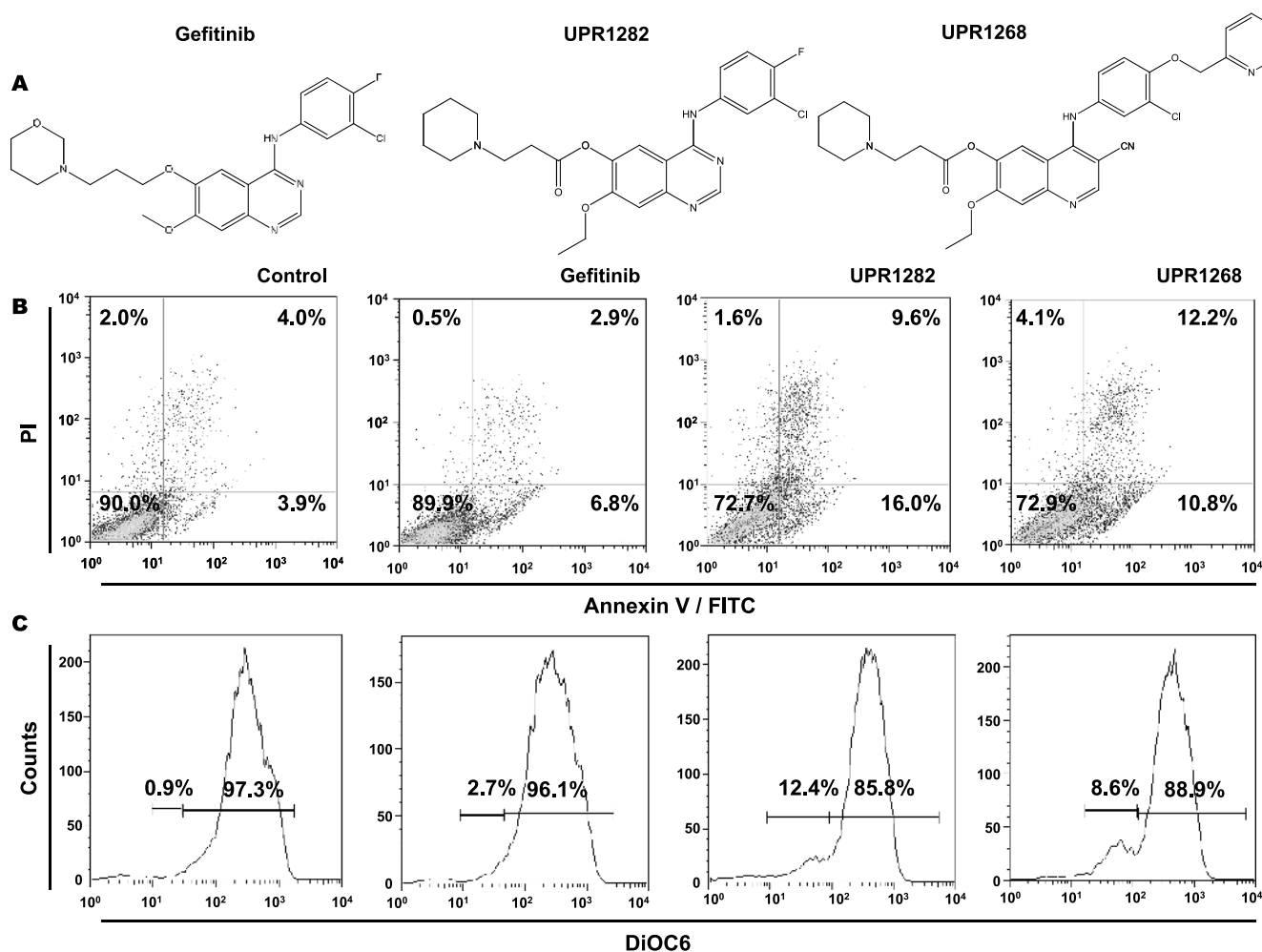


Figure 1. Molecular structure and apoptosis induction of EGFR TKIs in H1975 cells. (A) Molecular structure of gefitinib, UPR1282, and UPR1268. (B) Annexin V staining: 2×10^5 H1975 cells per well were treated for 24 hours with 0.1% DMSO, 1 μ M gefitinib, or UPR1282/UPR1268 at their respective IC_{50} s. Cells were then stained with Annexin V-FITC and PI, and samples were analyzed by flow cytometry using excitation/emission wavelengths of 488/525 and 488/675 nm for Annexin V and PI, respectively. (C) Mitochondrial membrane potential: 2×10^5 H1975 cells per well were treated for 24 hours with 0.1% DMSO, 1 μ M gefitinib, or UPR1282/UPR1268 at their respective IC_{50} s and then incubated with 40 nM DiOC₆. The samples were analyzed with the flow cytometer, and living cells were defined by size (FSC) and granularity (SSC).

profiling using short tandem repeats, which was performed by BaseClear (Leiden, The Netherlands) in August 2011.

Cell Growth Inhibition

Cell growth inhibition was assessed by sulforhodamine B assay according to the National Cancer Institute (NCI) protocol with slight modifications [23]. The pure compounds were initially dissolved in DMSO and tested in triplicates in the range of 0.01 to 20 μ M. The treatment was started on day 1 after plating, and cells were exposed to drugs for 72 hours. The control wells were exposed to 0.1% DMSO. After 72-hour treatment, 25 μ l of ice-cold 50% (wt/vol) trichloroacetic acid were added to each well for 60 minutes at 4°C. Then, the sulforhodamine B assay was performed, as described previously [24]. The optical density (OD) of each well was measured at 540 nm by TiterTek Multiskan MCC/340 (Flow Laboratories, Inc, Rockville, MD) 96-well plate reader. Values were corrected for background OD from wells containing medium only supplemented with 0.1% DMSO. The inhibition of cell viability was calculated with respect to control DMSO-treated cells based on the difference in OD at the beginning

(day 0) and after 72 hours of treatment (day 3), according to the NCI protocol [23]. The 50% growth inhibitory concentration (IC_{50}) was expressed as the concentration inhibiting 50% of the growth of drug-treated cells relative to the DMSO-only-treated ones and calculated by nonlinear least squares curve fitting (GraphPad Prism, Intuitive Software for Science, San Diego, CA). Microscopic images of H1975 cells exposed to 0.1% DMSO or UPR1282 and UPR1268 at their IC_{50} s were taken immediately before (time zero) and after 72 hours of treatment by Leica DFC345 FX microscope (Leica Microsystems GmbH, Wetzlar, Germany; Figure W1).

Analysis of Apoptosis with Annexin V Staining and Mitochondrial Membrane Potential

For the Annexin V staining, H1975 cells were plated at a density of 2×10^5 cells/well in six-well plates. After 24 hours, 1 μ M gefitinib or UPR1282 and UPR1268 at their respective IC_{50} s were added and cells were then incubated for 24 hours. DMSO (0.1%) was added to the control wells. Cells were then trypsinized, harvested, transferred to test tubes (12 \times 75 mm), and centrifuged at 1200 rpm for 10 minutes.

The pellets were resuspended in 100 μ l of ice-cold binding buffer (0.1 M HEPES/NaOH (pH 7.4), 1.4 M NaCl, and 25 μ M CaCl₂). Annexin staining was performed according to the manufacturer's protocol (Annexin V–Fluorescein Isothiocyanate (FITC) Apoptosis Detection Kit I; Becton Dickinson, San Jose, CA), with minor modifications as previously described [25]. Cells were stained with both 5 μ l of Annexin V–FITC and 5 μ l of propidium iodide (PI) and incubated for 15 minutes at room temperature in the dark before adding 400 μ l of binding buffer to each tube. Samples were then analyzed by flow cytometry in FACSCalibur Flow Cytometer (Becton Dickinson) and the results were processed using FACSDiva 6.0 software (Becton Dickinson). A total of 10,000 events were collected using excitation/emission wavelengths of 488/525 and 488/675 nm for Annexin V and PI, respectively.

For the analysis of the mitochondrial membrane potential, H1975 cells treated as described above were harvested and transferred to flow cytometer's tubes and incubated in phosphate-buffered saline (PBS) supplemented with 40 nM DiOC₆ (Sigma) for 20 minutes at 37°C in the dark. Then, cells were washed with PBS and the samples were analyzed with the FACSCalibur Flow Cytometer and the FACSDiva 6.0 software. A total of 10,000 events were acquired and living cells were defined by size [forward scatter (FSC)] and granularity [side scatter (SSC)].

Genetic Characterization of Cancer Cells

DNA was isolated from 10⁶ cells per cell line, using the MiniDNA Kit (Qiagen, Hilden, Germany). DNA yields and purity were checked at 260 to 280 nm with NanoDrop 1000 Detector (NanoDrop Technologies, Wilmington, DE). Nested PCR to amplify EGFR (exons 18–21) and K-Ras (exons 1–2) and sequencing of PCR products on an ABI 3100 genetic analyzer (Applied Biosystems, Foster City, CA) were performed as described previously [24]. The AKT1-SNP4 G/A (dbSNP-ID:rs1130233) polymorphism was studied using a Taqman probe-based assay with specific primers and probes obtained from Applied Biosystems (C_7489835_10). PCRs were performed using 20 ng of DNA diluted in 5.94 μ l of DNase-RNase-free water, with 6.25 μ l of TaqMan Universal PCR Master Mix and 0.31 μ l of the mix, including the primers and probes, in a total volume of 12.5 μ l. After thermal cycling, the 7500HT instrument determined the allelic content of each sample in the plate by reading the generated fluorescence, using the SDS 2.0 software.

Quantitative Real-Time Reverse Transcription–PCR

Total RNA was isolated using the TRI Reagent LS (Invitrogen, Carlsbad, CA). One microgram of RNA was retro-transcribed using the DyNAmo cDNA Synthesis Kit (Thermo Scientific, Vantaa, Finland), according to the manufacturer's instructions. Primers and probes to specifically amplify CD133 and E-cadherin were obtained from Applied Biosystems Assay-on-Demand Gene expression products (Hs00901885_m1, Hs01023894_m1). The quantitative real-time PCR was performed in a 25- μ l reaction volume containing TaqMan Universal Master Mix (Applied Biosystems). All reactions were performed in triplicate using the ABI Prism 7500 sequence detection system instrument (Applied Biosystems). Samples were amplified using the following thermal profile: 50°C for 2 minutes, 95°C for 10 minutes, 40 cycles of denaturation at 95°C for 15 seconds followed by annealing and extension at 60°C for 1 minute. A validation experiment was performed to demonstrate that the efficiencies of the targets (E-cadherin and CD133) and reference (β -actin) gene amplifications were approximately equal, using a standard curve method with several dilutions of

the cDNA sample from untreated control H1975 cells. An ideal slope should be -3.32 ; the values of the slopes of cDNA calibrator relative to threshold cycle (C_T) for the target genes revealed PCR efficiencies above 95%. Amplifications were normalized to β -actin (TaqMan β -Actin Detection Reagents, Part No. 401846). The fold change was calculated by the $\Delta\Delta C_T$ method and results were plotted as $2^{-\Delta\Delta C_T}$.

Western Blot

After 1 hour of exposure to 0.1% DMSO or different concentrations of gefitinib (0.01 to 10 μ M) and UPR1282 and UPR1268 (both from 0.001 to 10 μ M), H1975 cells were stimulated for 5 minutes with EGF (50 μ g/ml) and then lysed by RIPA buffer supplemented with protease and phosphatase inhibitor cocktails. Procedures for protein extraction, solubilization, and protein analysis by one-dimensional polyacrylamide gel electrophoresis (PAGE) are described elsewhere [26]. Samples of 40 to 50 μ g of proteins were resolved by 10% sodium dodecyl sulfate–PAGE and transferred to polyvinylidene difluoride (PVDF) membranes. The following antibodies were used (Bioké, Leiden, The Netherlands): polyclonal anti-phospho-EGFR (Tyr¹⁰⁶⁸) [1:1000 in 1:1 solution of Rockland (Rockland Inc, Philadelphia, PA) with PBS supplemented with 0.05% Tween 20], monoclonal anti-EGFR (1:1000), polyclonal anti-phospho-Akt (Ser⁴⁷³; 1:1000), monoclonal anti-Akt (1:1000), polyclonal anti-phospho-p44/42 (Thr²⁰²/Tyr²⁰⁴; 1:1000), and monoclonal anti-p44/42 (1:1000). As secondary antibodies, goat anti-mouse InfraRedDye (1:10,000, 800CW; #926-32210 and 680CW; #926-32220; Westburg, Leusden, The Netherlands) or goat anti-rabbit InfraRedDye (1:10,000, 800CW; #926-32211 and 680CW; #926-32221) were used. As a loading control, expression of β -actin was determined using an antibody against β -actin in stripped membranes (1:10,000; Millipore Bioscience Research Agents, Temecula, CA). Fluorescent proteins were detected by an Odyssey Infrared Imager (LI-COR Biosciences, Lincoln, NE), at 84- μ m resolution, 0-mm offset, using high-quality settings.

Peptide Substrate Array

To evaluate modulation of kinase activity by gefitinib, canertinib, and UPR1282 in H1975 cells and tissues from xenograft models, we profiled lysates from the cells and the tumors by using a kinase peptide substrate array (PamChip; PamGene International, 's-Hertogenbosch, The Netherlands) as previously described [27]. This array contains 144 peptides consisting of 15 amino acids including a tyrosine, usually in the middle of the peptide. The 13 COOH-terminal amino acids of each peptide correspond to known or putative phosphorylation sites in a variety of human proteins. The samples were lysed for 20 minutes at 4°C by M-PER containing phosphatase and protease inhibitors (Thermo Scientific, Rockford, IL). Lysates were centrifuged for 15 minutes at 10,000g; the supernatant was collected and stored at -80°C . Forty microliters of control sample mix for the kinase activity array was subsequently prepared by using reaction buffer containing 1 \times ABL buffer (Westburg), 100 μ M adenosine triphosphate (Sigma-Aldrich), fluorescein-labeled antibody PY20 (Exalpha, Maynard, MA), 5 μ g of (lysate) protein, and DMSO. Kinase inhibition was measured by the addition of 25 μ M gefitinib, 25 μ M canertinib, or 25 μ M UPR1282 (final drug concentrations; DMSO concentration in all samples, 2.5%). After blocking the arrays with 2% BSA and subsequent loading of the sample mix onto the arrays, incubation (at 30°C) was started for 60 cycles using a PamStation 12 instrument. Repeated fluorescent imaging of each array was performed with a 12-bit charge-coupled device (CCD) camera, monitoring fluorescence intensities in real time. Spot

intensity at each time point was quantified (and corrected for local background), and the resulting time-resolved curves were fit to calculate the initial phosphorylation rate (V_{ini}) using specific kinetic algorithms and appropriate statistical methods, by Bionavigator software version 5.1 (PamGene International).

In Vitro Migration Assay (Wound-Healing Assay)

Migration was evaluated using the LeicaDMI300B migration station (Leica Microsystems) integrated with the Scratch Assay 6.1 software (Digital Cell Imaging Labs, Keerbergen, Belgium). Thirty thousand H1975 cells per well were plated onto 96-well plates, and after 24 hours, artificial wound tracks were created by scraping with a specific scratcher within the confluent monolayers. After removal of the detached cells by gently washing with PBS, the medium was replaced and the cells were exposed to 0.1% DMSO, 1 μ M gefitinib, or UPR1282 and UPR1268 at their respective IC_{50} s. The ability of the cells to migrate into the wound area was assessed by comparing the pixels of the wound tracks in the images taken at the beginning of the exposure (time zero) with those taken after 4, 6, 8, and 24 hours [28].

Activity on H1975-Derived Tumor Spheres

A subpopulation of lung cancer stem-like cells were isolated by culturing 1.5×10^4 H1975 cells per well in serum-free insulin-transferrin-selenium (1:1000; Gibco, Invitrogen) supplemented with Dulbecco's modified Eagle's medium/F12 + GlutaMAX-I (1:1), in 24-well ultralow adherent plates (Corning Incorporated, Corning, NY), according to the manufacturers' protocol, as previously described [28]. The spheroids were generated for 20 to 25 days and then harvested for the growth inhibition studies in 96-well plates, as well as for RNA isolation. After checking their growth and stability, H1975 spheroids were treated with 0.1% DMSO, 1 μ M gefitinib, as well as UPR1282 or UPR1268 at their IC_{50} s. Each well was scanned at 0, 24, 48, and 72 hours of treatment. The effects of the drugs were evaluated in term of changes in the volume and in the total number of spheroids using the inverted phase contrast microscope LeicaDMI300B integrated with the Universal Grab 6.3 software (Digital Cell Imaging Labs). The volume of the spheroids (V) was calculated as volume of spheres having as diameter the average of the maximum and minimum diameters [$D = (D_{max} + D_{min})/2$; $V = 4/3\pi(D/2)^3$] obtained from the images by measurement with ImageJ software (ImageJ 1.45s; by Wayne Rasband, National Institutes of Health, Bethesda, MD).

Tumor Xenografts

All experiments involving animals were performed in accordance with Guiding Principles in the Care and Use of Animals (DL116/92). Twenty-four BALB/c-Nude female mice (Charles River Laboratories, Calco, Italy) were housed in a protected unit for immunodeficient animals with 12-hour light/dark cycles and provided with sterilized food and water *ad libitum*. At the time of xenograft experiments, mice were 7 weeks old and weighted about 20 g. Two hundred microliters of matrigel (BD Biosciences, Franklin Lakes, NJ) and sterile PBS (1:1) containing 1×10^7 H1975 cells were subcutaneously injected on the right flank of each mouse (using a 1-ml syringe, needle G25). The injected cells generated a solid tumor localized in correspondence of injection site. When tumor volume reached an average size of 150 to 200 mm^3 , 1 month after injection, animals were randomized into

four groups and treated for 25 days. At the end of the treatment, mice were killed by cervical dislocation and tumors were collected and stored at $-80^\circ C$ until used for peptide kinase array or formalin fixed for hematoxylin-eosin staining or immunohistochemistry.

Treatment and Tumor Measurement

Gefitinib, canertinib, and UPR1282 were orally administered, 5 days/week, at the dosage of 25 mg/kg in 1% Tween 80, while the animals in the control group received oral gavage of vehicle alone.

Tumor xenografts were measured twice a week and tumor volume was calculated using the formula: $(length \times width^2)/2$. Final data are expressed as percentage of volume increase: $tumor\ volume/pre-treatment\ tumor\ volume \times 100$.

Sections of formalin-fixed, paraffin-embedded xenograft tumors were stained with hematoxylin and eosin for initial histopathologic examination to confirm the presence of NSCLC cells. This is a widely used, two-stage stain for cells in which hematoxylin is followed by a counterstain of red eosin so that the nuclei stain a deep blue-black and the cytoplasm stains pink. This staining allows the detection of focally multinucleated cells and mitotic figures within the tumors.

Immunohistochemistry

Tumor tissue sections were constructed using tissue biopsies obtained from three mice from the different groups included in recipient paraffin blocks. Before staining with the monoclonal antibody from the EGFR pharmDx Kit, the slides were deparaffinized using xylene and rehydrated in alcohol, as described previously [29]. Negative controls were obtained by replacement of primary antibody with buffer ($1 \times$ PBS). EGFR staining results were evaluated using a four-tier system including the analysis of both the number of positive cells and the staining intensity. All slides were reviewed by two independent observers who also evaluated the amount of tissue loss, background staining, and overall interpretability before the formal EGFR reactivity evaluation. Neoplastic cells were always uniformly stained, and positivity assessment was made by counting at least 2000 tumor representative cells.

Statistical Analysis

All experiments were performed in triplicate and repeated at least twice. Data were expressed as mean values \pm SD and analyzed using the two-tailed Student's t test or analysis of variance followed by the Bonferroni's multiple comparison test, using Prism 5.0 (GraphPad Software). The level of significance was set at $P < .05$.

Results

Antiproliferative and Cytotoxic Effects

The novel UPR1282 and UPR1268 compounds (Figure 1A) were evaluated in comparison to the first-generation EGFR TKI gefitinib for their ability to inhibit the growth and viability of different cell lines, including the gefitinib-resistant H1975 cell line harboring the T790M mutation (Table 1). The 4-(3-chloro-4-fluoroanilino)-7-ethoxyquinazolino derivative UPR1282 was significantly more active in comparison with gefitinib in the three tested NSCLC cell lines. In particular, UPR1282 was nine-fold more effective than gefitinib in inhibiting H1975 proliferation but only two-fold in the NSCLC cell lines A549 and Calu-1. Because of the approval of the

Table 1. Human Cancer Cell Line Characteristics and Sensitivity to EGFR TKIs.

| Cell Line | Histology | EGFR Status | K-Ras Status | AKT1 SNP4 | Gefitinib IC ₅₀ (μM) | UPR1282 IC ₅₀ (μM) | UPR1268 IC ₅₀ (μM) |
|-------------------|-------------------------|----------------|--------------|-----------|---------------------------------|-------------------------------|-------------------------------|
| H1975 (NSCLC) | Adenocarcinoma | L858R T790M | WT | GG | 11.7 ± 1.3 | 1.2 ± 0.5* | 0.6 ± 0.1* |
| A549 (NSCLC) | Adenocarcinoma | WT | Mut (G12S) | GA | 6.4 ± 0.8 | 3.4 ± 0.3* | 0.7 ± 0.1* |
| Calu-1 (NSCLC) | Squamous cell carcinoma | WT | Mut (G12C) | GG | 19.3 ± 1.2 | 8.6 ± 0.2* | 8.0 ± 0.5* |
| PANC-1 (PDAC) | Epithelioid carcinoma | WT | Mut (G12D) | AA | 7.6 ± 0.4 | 7.7 ± 1.1 | 5.6 ± 0.1* |
| MIA PaCa-2 (PDAC) | Carcinoma | WT | Mut (G12C) | AA | 14.1 ± 0.2 | 11.6 ± 0.3* | 2.4 ± 0.1* |

Data on determinants of gefitinib sensitivity in NSCLC cell lines have been published by Giovannetti et al. [24]. Mut, mutation; WT, wild type.

**P* < .05 with respect to gefitinib treatment.

EGFR TKI erlotinib in combination with gemcitabine [30], for the treatment of advanced PDAC, we also evaluated the biological activity of our compounds in PDAC cells. Our molecules were as active as gefitinib in inhibiting the proliferation of both PANC-1 and MIA PaCa-2 cells. Moreover, a 16-fold difference compared to gefitinib was observed with UPR1268 in H1975 cells. This compound was also nine- and two-fold more effective than gefitinib in reducing A549 and Calu-1 cell viability, respectively. Furthermore, in the PDAC cells MIA PaCa-2, the same compound showed a five- to six-fold increase in potency with respect to the first-generation EGFR TKI. The inhibition of H1975 cell proliferation was detected also microscopically after exposure of the cells to UPR1282 and UPR1268 at their IC₅₀s (Figure W1).

Apoptosis was investigated as potential mechanism of cell death induced by these compounds using cytofluorometric analysis of Annexin V staining and mitochondrial membrane potential. One micromolar gefitinib was chosen as treatment of reference, as it is the concentration more commonly used in the preclinical setting to reflect the mean blood concentration reached in NSCLC patients treated with the inhibitor. In apoptotic cells, the membrane phospholipid phosphatidylserine is translocated from the inner to the outer leaflet of the plasma membrane, thereby exposing phosphatidylserine to the external cellular environment. Annexin V labeled with the FITC fluorescent tag was used with flow cytometry to measure this

event. Moreover, because Annexin V staining precedes the loss of membrane integrity that accompanies the later stages of cell death resulting from either apoptotic or necrotic processes, we used the staining with Annexin V-FITC in conjunction with a live/dead dye such as PI to allow the identification of early apoptotic cells (PI negative, Annexin V-FITC positive) from late apoptotic/dead cells (PI positive, Annexin V-FITC positive). The 24-hour treatment with the novel molecules increased both events, as illustrated in Figure 1B. In particular, IC₅₀s of UPR1282 and UPR1268 increased the early apoptosis from 3.9 to 16.0 and 10.8% and the late apoptosis from 4.4 to 9.6 and 12.2%, respectively. Mitochondrial damage was assessed biochemically by measuring DiOC₆, a cationic dye that is released when the mitochondrial membrane potential is damaged. As shown by the representative histograms of cytofluorometric analysis in Figure 1C, a clear decrease in the binding of DiOC₆ was observed in H1975 cells treated for 24 hours with UPR1282 and UPR1268, as described above. Conversely, no differences were observed in cells treated with gefitinib compared to control cells that were exposed to 0.1% DMSO (Figure 1, B and C).

Inhibition of EGFR Autophosphorylation and Downstream Signaling Pathways

To get further insights into the mechanism of action of the new compounds compared to gefitinib, we investigated their effect on

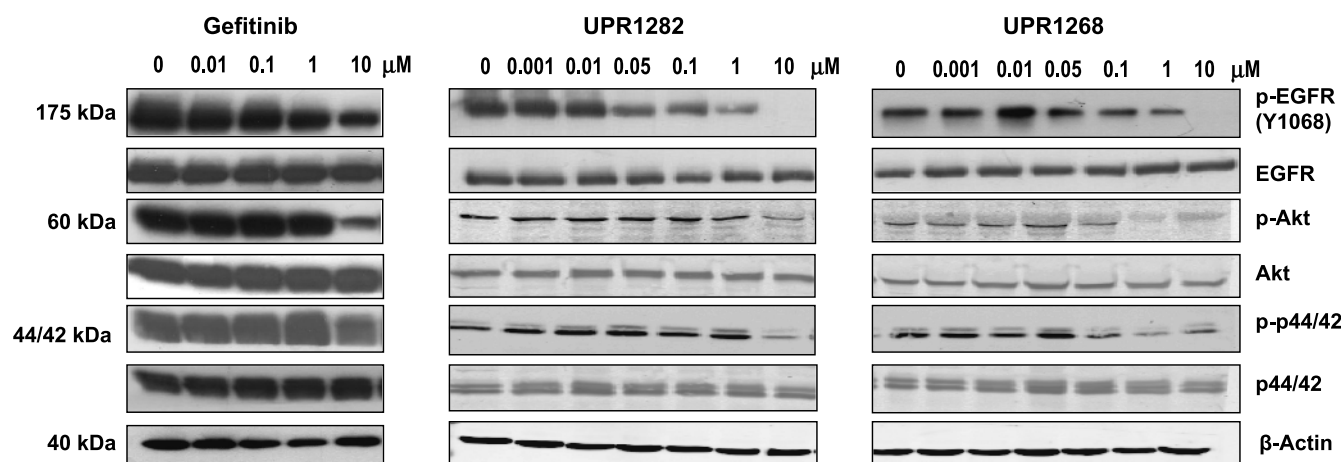


Figure 2. EGFR and downstream pathway phosphorylation analyses by Western blot; 1×10^6 H1975 cells per well were plated in six-well plates and, after 24 hours, were exposed for 1 hour to 0.01 to 10 μM gefitinib, 0.001 to 10 μM of both UPR1282 and UPR1268, or 0.1% DMSO (control). Stimulation with EGF (50 μg/ml) for 5 minutes was performed before protein extraction. Samples of 40 to 50 μg of proteins were resolved by 10% sodium dodecyl sulfate-PAGE and transferred to PVDF membranes. Fluorescent proteins were detected and analyzed by Odyssey Infrared Imager at 84-μm resolution, 0-mm offset, using high-quality settings. The immunoblot of gefitinib activity in H1975 cells has been previously published by Carmi et al. [10].

crucial phosphorylation pathways (Figure 2). A concentration-dependent inhibition of EGFR autophosphorylation in H1975 cells was observed after exposure to both UPR1282 and UPR1268, with IC_{50} of 0.08 and 0.15 μ M, respectively. A complete inhibition of EGFR phosphorylation was reached by both UPR compounds at the highest tested concentration (10 μ M). In the same experimental conditions, gefitinib only slightly reduced EGFR autophosphorylation at 10 μ M. As a consequence of the inhibition of the receptor, both our novel compounds affected the phosphorylation of the downstream signaling molecules p-Akt and p-p44/42, whereas gefitinib had a marginal effect on p-Akt at 10 μ M. Furthermore, we investigated alterations of core signaling pathways after exposure to UPR1282, in comparison with gefitinib and canertinib, using a recently established high-throughput kinase array [27]. In cell lysates, kinase activity profiling was performed in the absence and presence of 25 μ M gefitinib, canertinib, or UPR1282. Data of V_{ini} in treated cells were compared to the DMSO-treated ones and a total of 28, 43, and 21 kinases, linked to many peptide substrates, were identified with a percentage of inhibition of more than 66.6%, caused by gefitinib, canertinib, and UPR1282, including nine common targets (Table 2). Importantly, EGFR, ErbB2, and ErbB4 inhibition was observed as a consequence of each treatment.

EMT and Inhibition of Cellular Migration

Accumulating evidence suggests a critical role of EMT in epithelial cancer progression, invasion, and metastasis. Cell features, including cell-cell and cell-matrix interactions, are highly affected by EMT, and loss of intracellular cohesion, together with the disruption of extracellular matrix (ECM) and modifications of the cytoskeleton, has been related to increased cell motility and invasiveness [31]. The family of cadherins comprises molecules that are involved in cell-cell adhesion, and their deregulation may result in EMT and cell motility. Recent studies demonstrated the correlations between cell-cell contact and cytoplasmic signaling pathway activation or inhibition [32]. Wnt signaling has emerged as critical pathway in lung tumorigenesis through the β -catenin-mediated transcription of zinc-finger proteins such as Slug and Snail, in which expression is inversely correlated with E-cadherin transcription [33]. Destruction of E-cadherin by receptor tyrosine kinases and Ras pathway was demonstrated to cause release of β -catenin from disassembled junctions between epithelial cells and promote cell transformation [34]. Thus, E-cadherin was first investigated by reverse transcription (RT)-PCR as molecule related to cellular migration. Whereas gefitinib did not affect the level of E-cadherin mRNA in H1975 cells, the exposure to the novel irreversible inhibitors significantly increased its gene expression when compared to DMSO-treated cells (Figure 3A). Furthermore, to explore whether UPR1282 and UPR1268 affect cell migration, a scratch motility assay was performed in H1975 cells. Both molecules significantly reduced cell migration in comparison to the control, whereas gefitinib did not result in any effect (Figure 3, B and C).

Volume Reduction of H1975-Derived Tumor Spheres

Results from earlier studies illustrated that the sensitivity of two-dimensional monolayer cell cultures to anticancer drugs is different from that obtained in three-dimensional culture models [35]. Furthermore, the cancer stem cell (CSC) theory prompted to the reexamination of established views of tumor initiation, progression, and therapeutic resistance [36]. Recently, the use of serum-free medium has been reported to select cell populations harboring CSC-like characteristics,

Table 2. Kinase Activity Profiles of Gefitinib, Canertinib, and UPR1282 in H1975 Cells.

| Peptides | Gef | Can | UPR |
|-----------------|-----|-----|-----|
| ANXA1_14_26 | | X | |
| ANXA2_17_29 | X | X | |
| B3AT_39_51 | | | X |
| PGFRB_1014_1028 | | X | |
| CALM_95_107 | X | X | X |
| CBL_693_705 | | X | |
| CD3Z_116_128 | | X | |
| CD3Z_146_158 | | X | |
| CDK2_8_20 | | X | |
| DCX_109_121 | X | X | X |
| EGFR_1190_1202 | | X | X |
| EGFR_862_874 | X | | |
| EPHA4_589_601 | | X | X |
| EPHB1_771_783 | | X | |
| EPHB4_583_595 | X | | X |
| EPOR_361_373 | | X | X |
| ERBB2_870_882 | X | | |
| ERBB4_1181_1193 | | X | |
| ERBB4_1277_1289 | | X | |
| FAK1_569_581 | | | X |
| FAK2_572_584 | X | | |
| FES_706_718 | | X | |
| FGFR3_641_653 | | X | X |
| JAK1_1015_1027 | | X | |
| JAK2_563_577 | | X | |
| K2C6B_53_65 | X | X | X |
| K2C8_425_437 | | X | X |
| KSYK_518_530 | X | | |
| LCK_387_399 | | X | |
| MK01_180_192 | | X | X |
| MK10_216_228 | X | X | X |
| MK14_173_185 | | X | |
| NTRK1_489_501 | X | X | X |
| NTRK2_509_521 | X | X | X |
| ODPAT_291_303 | X | X | X |
| PP2AB_297_309 | X | | |
| PECA1_706_718 | | X | |
| PERL_458_470 | X | | X |
| PLCG1_1246_1258 | | X | |
| PLCG1_776_788 | | X | |
| PRGR_545_557 | X | | |
| PRGR_786_798 | X | | |
| RASA1_453_465 | X | X | X |
| RBL2_99_111 | X | X | |
| RON_1346_1358 | X | X | |
| RON_1353_1365 | | X | |
| STAT1_694_706 | X | X | |
| STAT4_714_726 | X | X | |
| TNNT1_2_14 | X | | X |
| TYRO3_679_691 | X | X | |
| VGFR1_1046_1058 | X | X | |
| VGFR1_1162_1174 | | X | |
| VGFR1_1235_1247 | X | X | |
| VGFR2_1046_1058 | | X | |
| VGFR2_1052_1064 | X | X | |
| VGFR2_1168_1180 | X | | X |
| VGFR2_1207_1219 | X | X | X |
| VGFR3_1061_1073 | X | X | |

Gef, gefitinib; Can, canertinib; UPR, UPR1282; X, percentage of kinase inhibition of more than 66.6% in comparison with untreated H1975 cells. The acronyms refer to peptides/proteins from <http://www.expasy.org/uniprot/>.

including self-renewal and differentiation into heterogeneous lineages of cancer cells [37]. This experimental approach represents the best strategy so far to obtain the expansion of the tumorigenic cell subpopulation. Furthermore, recent studies unraveled the importance of CSC CD133-positive cells in tumorigenicity and chemoresistance of lung cancer [38]. Thus, to determine whether three-dimensional systems, enriched with CSC-like properties, could be affected by our compounds, we developed tumor spheres from H1975 cells that, after

20 to 25 days of culture, reached a size of approximately 400 to 500 μm in diameter (Figure 4A). We evaluated then by RT-PCR the level of CD133 mRNA as marker of stemness, comparing adherent cells *versus* tumor spheres. In agreement with previous studies, a significantly higher expression of CD133 mRNA was observed in tumor spheres when compared to adherent cells (Figure 4B). When treated with gefitinib or the novel TKIs, the total number of H1975 spheroids was not affected. However, the treatment with the novel inhibitors significantly reduced tumor sphere volume when compared to the time zero of treatment (Figure 4, C and D). In contrast, gefitinib treatment did not affect the growth of these three-dimensional spheroidal systems (data not shown). Furthermore, the exposure of tumor spheres to UPR1282 and UPR1268 significantly reduced CD133 gene expression (Figure 4E), whereas the treatment with gefitinib did not cause any change in CD133 mRNA when compared to DMSO-only-treated spheroids (data not shown).

Tumor Shrinkage in H1975 Xenograft Model and Signaling Pathway Inhibition in Tumor Tissue

To evaluate the potential of our compounds *in vivo*, we tested the effects of UPR1282 in comparison with gefitinib and canertinib

(H1975 $\text{IC}_{50} = 2.4 \mu\text{M}$) in H1975-derived xenografts. When tumors were well established and reached an average volume of 150 to 200 mm^3 , the mice were randomized into four treatment groups receiving gefitinib, canertinib, UPR1282, or vehicle. The treatment with either canertinib or UPR1282 caused tumor shrinkage, whereas gefitinib did not affect tumor growth in comparison to the control group (Figure 5A). Of note, canertinib significantly inhibited tumor growth after 21 days of treatment. However, this shrinkage was accompanied by a significant reduction of animal body weight compared to untreated animals as well as to mice treated with UPR1282 (Figure 5B). Immunohistochemistry was then performed on three tumor tissues per group and EGFR was evaluated as marker to confirm the origin of the tumor from our human lung cancer cells (Figure 5C). To evaluate the activity of our novel drug in tumor tissues, we performed an additional kinase activity profiling in tissue lysates, in the absence or presence of 25 μM UPR1282. Data of V_{ini} in treated lysates from H1975 xenograft specimens, which according to hematoxylin-eosin staining in Figure 5C contained more than 80% of tumor cells, were compared to data obtained from the treatment of H1975 cell lysate. This array identified a strong percentage of inhibition (i.e., more than 66.6%) of 17 and 21 kinases in tissue and cell lysates, respectively, including seven

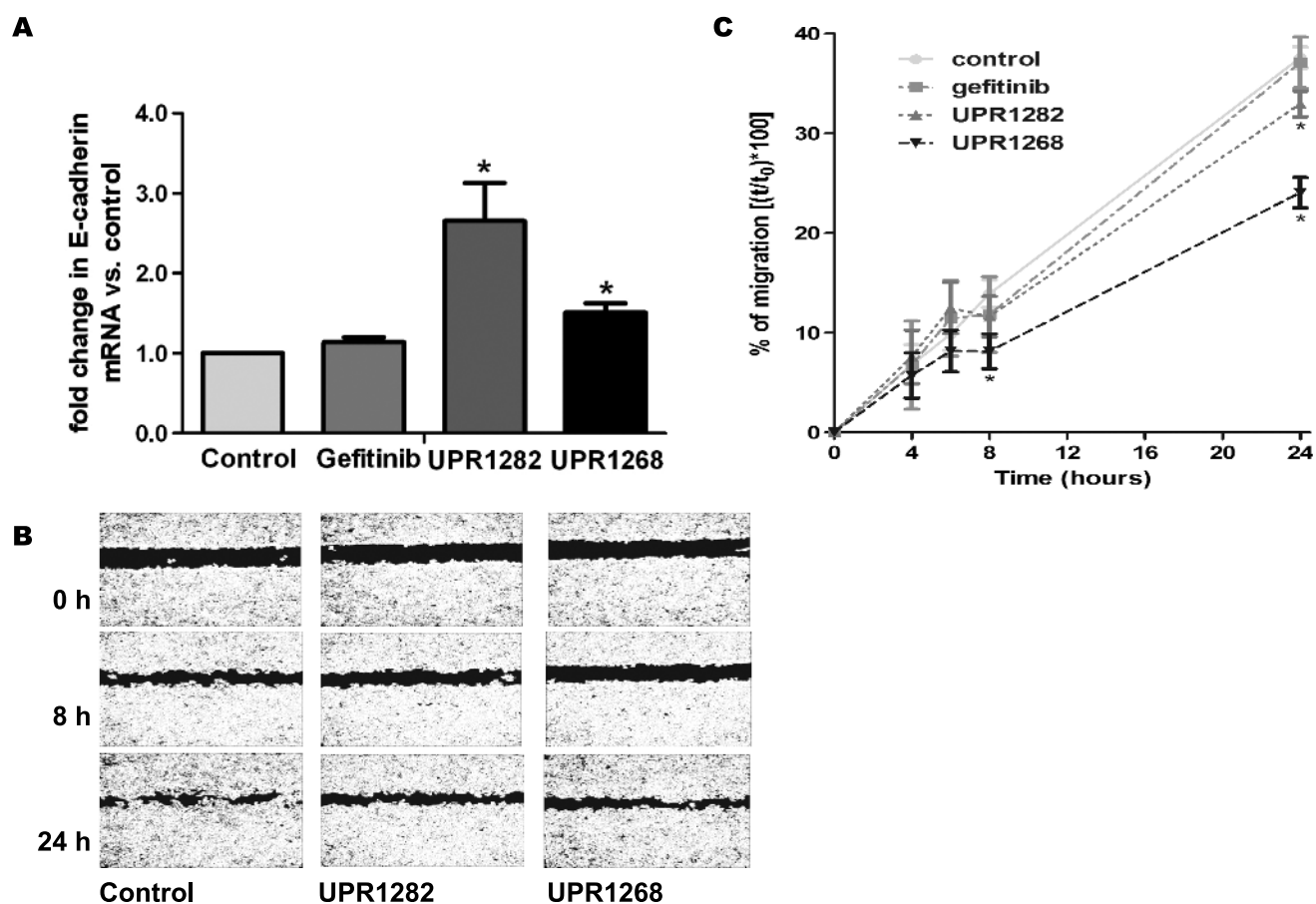


Figure 3. Effects of EGFR TKIs on H1975 cell migration. (A) E-cadherin evaluation by quantitative RT-PCR after exposure of H1975 cells to 1 μM gefitinib or UPR1282 and UPR1268 to their respective IC_{50} s for 24 hours. (B) Representative images of the wound tracks (created 24 hours after plating 3×10^5 H1975 cells per well) in time with different treatments. The control is represented by cells exposed to 0.1% DMSO. (C) Comparison of the effect of the different treatments on the percentage of cell migration. After 24 hours since plating, cells were treated with 0.1% DMSO, 1 μM gefitinib, 1.2 μM UPR1282, or 0.6 μM UPR1268. The wound areas were measured after 0, 4, 6, 8, and 24 hours of treatment. The percentages of migration are referred to the time zero measurements and represent the averages of four replicates repeated in three independent experiments.

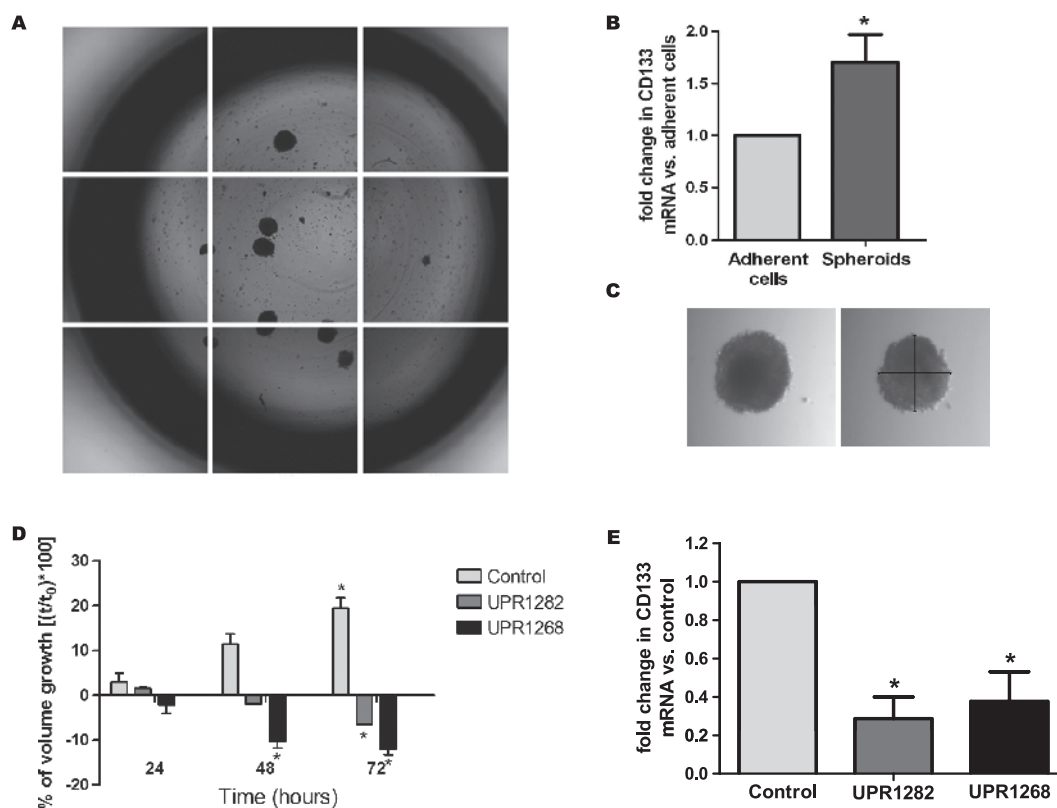


Figure 4. Effects of EGFR TKIs on H1975 grown as spheroids. (A) Composite representative image of an experimental well containing several spheroids. (B) Comparison of CD133 mRNA by quantitative RT-PCR in H1975 adherent cells *versus* tumor spheres. The fold change of CD133 mRNA in spheroids was calculated using the $2^{-\Delta\Delta CT}$ method relative to adherent cells used as control. (C) Representative image of diameter measurement in the evaluation of spheroid volume. (D) After 20 to 25 days, H1975 spheroids were treated with 1 μ M gefitinib as well as with UPR1282 and UPR1268 at their IC₅₀s. The volume of the spheroids was measured at 24-, 48-, and 72-hour treatment and normalized to the volume of the spheroids at time zero treatment. (E) CD133 evaluation by quantitative PCR after exposure of tumor spheres to 1 μ M gefitinib or to UPR1282 and UPR1268 at their IC₅₀s for 24 hours.

common targets (Figure 5D). Importantly, EGFR inhibition by UPR1282 was confirmed by the peptide substrate array in both tissue and cells, confirming its powerful activity on this target.

Discussion

The present study demonstrates the activity of novel EGFR irreversible inhibitors against tumor cells, including *in vitro* and *in vivo* models of EGFR T790M NSCLC. Moreover, we evaluated several molecular mechanisms underlying the abilities of these novel compounds to effectively antagonize NSCLC aggressive and invasive behavior.

Molecular targeting of EGFR with the first-generation reversible TKIs gefitinib and erlotinib is now an established therapeutic option in advanced NSCLC patients who harbor activating mutations of the receptor [39]. However, the emerging acquired resistance together with the low survival benefit prompts further studies to improve this therapeutic approach. The necessity to overcome the resistance due to the T790M secondary mutation of EGFR led to the development of several second-generation irreversible TKIs of this target [3]. We recently synthesized a series of novel 3-aminopropanamide compounds that demonstrated to be active against H1975 NSCLC cells harboring the EGFR T790M mutation by irreversible binding to the receptor following intracellular activation to a cysteine-trapping chemical species [22]. The present study demonstrates that the two most promising com-

pounds inhibit cell proliferation and induce apoptosis in different NSCLC cell lines at significantly lower concentration than gefitinib. Because the EGFR TKI erlotinib has been approved for the treatment of advanced PDAC in combination with gemcitabine [30], we also evaluated the new molecules in PANC-1 and MIA PaCa-2 cells. In these cell lines, both our compounds were as active as gefitinib or even more active than the first-generation EGFR TKI. However, the very slight increase in survival obtained with the use of erlotinib [40] and the recent success of multicombinatorial approaches with conventional cytotoxic drugs reduce the impact of EGFR TKIs in the treatment of PDAC [41].

As expected on the basis of their anti-EGFR activity, the main downstream mediators of the EGFR signal transduction pathways (p-Akt and p-p44/42) were also affected by our novel compounds. However, despite EGFR inhibition was already detectable by Western blot in the nanomolar range of concentrations, the downstream signaling molecules were slightly inhibited at 1 μ M, particularly by UPR1268, and more clearly at the highest used concentration (10 μ M) for both the inhibitors. Furthermore, using a commercially available 144-peptide array, we detected other tyrosine kinases affected by UPR1282. The restricted subset of the peptides spotted on the array, together with the limited specificity and the use of lysates that cannot reproduce sub-cellular compartmentalization and protein docking or scaffolding, represent the main interdiction of this study [42]. However, several

additional tyrosine kinases that were significantly inhibited by UPR1282, including the fibroblast growth factor receptor 3, whose up-regulation has been correlated to radioresistance in squamous cell carcinoma, were identified [43]. Of note, EphB4 and the focal adhesion kinase 1 (FAK1), which are both involved in the neoplastic transformation process, were also inhibited by UPR1282 in H1975 cells [44,45]. Additionally, the treatment of the cell lysates with UPR1282 also inhibited c-Met, in which amplification represents the second cause of acquired resistance to the treatment with EGFR TKIs. In particular, the activity of the receptor was reduced by around 53% by UPR1282. Importantly, many kinases, including the previously mentioned, had relevant (although not always below the 66.6% threshold) levels of inhibition in both H1975 cell line and xenografts exposed to UPR1282.

These results potentially extend the use of UPR1282 to the treatment of NSCLCs that harbor mechanisms of resistance different than the EGFR T790M mutation.

The invasive and metastatic capacity of tumor cells constitute two pivotal mechanisms of malignant tumor development. The poor prognosis of lung cancer is related to strong metastasis potential, which is directly correlated with EMT [33]. The transformation of epithelial cells to motile, invasive, and migratory mesenchymal cells is the major feature of such process. Cell adhesion and detachment are regulated by interactions between cell-cell and cell-ECM that coordinate the invasive mechanism [46]. Several classes of proteins participate to invasive cancer phenotype. Recent studies reported the loss of function of the cadherin adhesion complex, and in particular E-cadherin, as hallmark

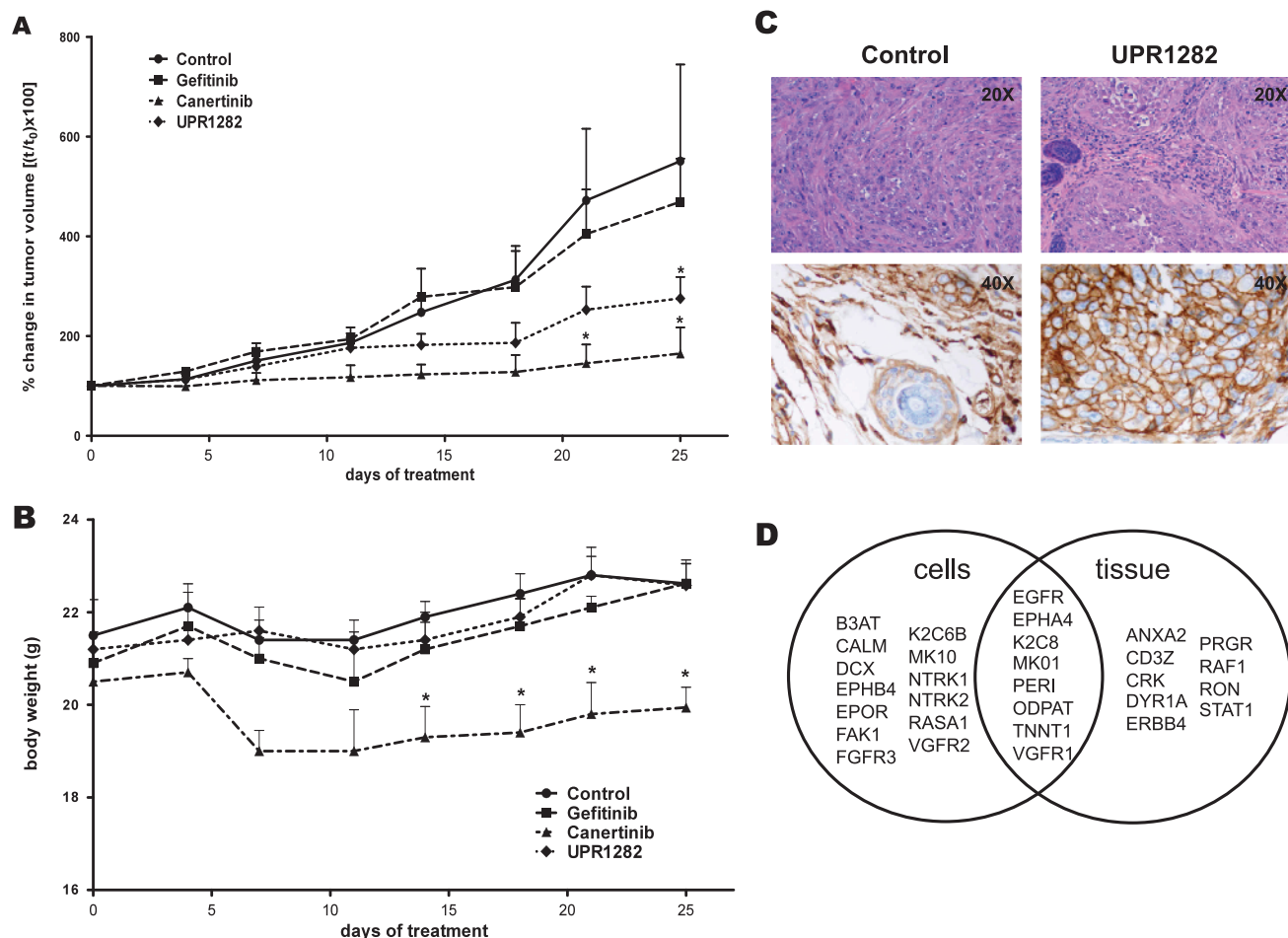


Figure 5. Effects of EGFR TKIs in xenograft models. (A) Effect of treatments with reversible and irreversible TKIs on tumor growth in a human NSCLC xenograft model. H1975 cells were suspended in a matrigel and sterile PBS (1:1) and implanted subcutaneously (right flank) on female BALB/c-Nude mice. Tumors were allowed to grow for 1 month, and the treatments started when they reached an average volume of 150 to 200 mm³. Vehicle, gefitinib, canertinib, or UPR1282 were administered orally 5 days per week, at a dosage of 25 mg/kg, for all the duration of the study. Data are expressed as percentage of change in tumor volume \pm SEM. (B) Effect of the chronic treatment of mice with vehicle, gefitinib, canertinib, or UPR1282 administered orally 5 days per week, at a dosage of 25 mg/kg on animal body weight. Data are expressed as percentage of change in tumor volume \pm SEM. (C) Representative tumor xenograft staining with hematoxylin and eosin and immunohistochemistry for EGFR of tissues from xenografts from control and UPR1282-treated groups. (D) Venn diagram of kinase profiles obtained from cells and tissue lysates treated with 25 μ M UPR1282. After loading of the sample mix onto the arrays, incubation (at 30°C) was started for 60 cycles utilizing a PamStation 12 instrument. Repeated fluorescent imaging of each array was performed to monitor fluorescence intensities in real time. Spot intensity was quantified and the resulting time-resolved curves were fit to calculate the initial phosphorylation rate (V_{ini}) using specific kinetic algorithms and appropriate statistical methods. Kinases that were identified to be inhibited more than 66.6% compared to DMSO-treated lysates of both cells and tissues are plotted in the Venn diagram.

of EMT that leads to increased proliferation, invasiveness, and metastasis [47]. Thus, we investigated whether the exposure to UPR1282 or UPR1268 might affect E-cadherin gene expression. Whereas treatment with gefitinib did not affect the level of mRNA coding for E-cadherin in H1975 cells, a significant increase in its gene expression was observed after exposure to our novel compounds. Furthermore, since recent studies demonstrated that EGF modifies cell-ECM adhesion [48], we tested whether our compounds might affect migration of EGFR T790M H1975 cells. Differently from what was observed after exposure to gefitinib, the novel 3-aminopropanamide compounds significantly reduced cell migration after few hours of treatment, as detected by the wound-healing assay. Such reduction in cell motility agrees with previous evidence on FAK inhibition and increased E-cadherin gene expression.

Accumulating evidence suggests that specific subpopulations of cancer cells within the bulk of tumors undergo different degree of EMT, and this process has been related with the acquisition of stem cell-like characteristics. Both EMT and stemness are implicated in the pathogenesis and chemoresistance of heterogeneous malignant tumors [21,49]. Treatment strategies for the elimination of cancer, therefore, need to consider the presence of CSCs. Sphere assay has proven to be an excellent technique to isolate CSCs and several studies demonstrated that the three-dimensional aggregates can contain different cell proliferation and metabolic gradients, such as an outer rim of viable and actively proliferating cells and an inner necrotic region [35]. Thus, after generating tumor spheres that overexpress the stem/initiating cell marker CD133, we explored whether our novel EGFR TKIs affected spheroid growth. Conversely to gefitinib, both the 3-aminopropanamide derivatives significantly reduced tumor sphere dimensions. Furthermore, we demonstrated that the level of CD133 mRNA was reduced after exposure to UPR1282 and UPR1268 [37,50].

The evaluation of the activity of UPR1282 was also extended to xenograft models of EGFR T790M NSCLC. The chronic administration of UPR1282 in athymic mice was well tolerated and produced significant inhibition of tumor growth, which might result from inhibition of both EGFR and downstream kinase activities. Of note, whereas tumor shrinkage induced by canertinib treatment was accompanied by significant toxicity, UPR1282 did not induce significant loss of body weight and toxicity even after a prolonged treatment. This might be, at least in part, related to the masking of acrylamide warhead that results in reduced risk of covalent interaction with off-target molecules [22].

In conclusion, our 3-aminopropanamide irreversible EGFR TKIs seem very promising anticancer agents by attacking different key mechanisms involved in the resistance of NSCLC cells to the first-generation EGFR TKIs gefitinib and erlotinib, including the EMT process. These data should prompt future trials that will give the ultimate proof of the utility of these novel anticancer agents for the treatment of lung cancer.

References

- Govindan R, Page N, Morgensztern D, Read W, Tierney R, Vlahiotis A, Spitznagel EL, and Piccirillo J (2006). Changing epidemiology of small-cell lung cancer in the United States over the last 30 years: analysis of the surveillance, epidemiologic, and end results database. *J Clin Oncol* **24**(28), 4539–4544.
- Hoang T and Schiller JH (2002). Advanced NSCLC: from cytotoxic systemic chemotherapy to molecularly targeted therapy. *Expert Rev Anticancer Ther* **2**(4), 393–401.
- Galvani E, Alfieri R, Giovannetti E, Cavazzoni A, La Monica S, Galetti M, Fumarola C, Bonelli M, Mor M, Tiseo M, et al. (2013). Epidermal growth factor receptor tyrosine kinase inhibitors: current status and future perspectives in the development of novel irreversible inhibitors for the treatment of mutant non-small cell lung cancer. *Curr Pharm Des* **19**(5), 818–832.
- Olayioye MA, Neve RM, Lane HA, and Hynes NE (2000). The ErbB signaling network: receptor heterodimerization in development and cancer. *EMBO J* **19**(13), 3159–3167.
- Ciardiello F and Tortora G (2008). EGFR antagonists in cancer treatment. *N Engl J Med* **358**(11), 1160–1174.
- Pao W, Miller VA, Politi KA, Riely GJ, Somwar R, Zakowski MF, Kris MG, and Varmus H (2005). Acquired resistance of lung adenocarcinomas to gefitinib or erlotinib is associated with a second mutation in the EGFR kinase domain. *PLoS Med* **2**(3), e73.
- Suda K, Onozato R, Yatabe Y, and Mitsudomi T (2009). EGFR T790M mutation: a double role in lung cancer cell survival? *J Thorac Oncol* **4**(1), 1–4.
- Engelman JA, Zejnullahu K, Mitsudomi T, Song Y, Hyland C, Park JO, Lindeman N, Gale CM, Zhao X, Christensen J, et al. (2007). MET amplification leads to gefitinib resistance in lung cancer by activating ERBB3 signaling. *Science* **316**(5827), 1039–1043.
- Bean J, Brennan C, Shih J-Y, Riely G, Viale A, Wang L, Chitale D, Motoi N, Szoke J, Broderick S, et al. (2007). MET amplification occurs with or without T790M mutations in EGFR mutant lung tumors with acquired resistance to gefitinib or erlotinib. *Proc Natl Acad Sci USA* **104**(52), 20932–20937.
- Carmi C, Cavazzoni A, Vezzosi S, Bordi F, Vacondio F, Silva C, Rivara S, Lodola A, Alfieri RR, La Monica S, et al. (2010). Novel irreversible epidermal growth factor receptor inhibitors by chemical modulation of the cysteine-trap portion. *J Med Chem* **53**(5), 2038–2050.
- Wu C-H, Coumar MS, Chu C-Y, Lin W-H, Chen Y-R, Chen C-T, Shiao H-Y, Rafi S, Wang S-Y, Hsu H, et al. (2010). Design and synthesis of tetrahydropyridothieno[2,3-*d*]pyrimidine scaffold based epidermal growth factor receptor (EGFR) kinase inhibitors: the role of side chain chirality and Michael acceptor group for maximal potency. *J Med Chem* **53**(20), 7316–7326.
- Cha MY, Lee K-O, Kim JW, Lee CG, Song JY, Kim YH, Lee GS, Park SB, and Kim MS (2009). Discovery of a novel Her-1/Her-2 dual tyrosine kinase inhibitor for the treatment of Her-1 selective inhibitor-resistant non-small cell lung cancer. *J Med Chem* **52**(21), 6880–6888.
- Ding K, Zhang L, Xu S, Luo J, Lu X, Xu T, Liu Y, Tu Z, Xu Y, Ren X, et al. (2012). Design, synthesis and biological evaluation of novel conformationally constrained inhibitors targeting epidermal growth factor receptor T790M mutant. *J Med Chem* **55**(6), 2711–2723.
- Smaill JB, Rewcastle GW, Loo JA, Greis KD, Chan OH, Reyner EL, Lipka E, Showalter HD, Vincent PW, Elliott WL, et al. (2000). Tyrosine kinase inhibitors. 17. Irreversible inhibitors of the epidermal growth factor receptor: 4-(phenylamino)quinazoline- and 4-(phenylamino)pyrido[3,2-*d*]pyrimidine-6-acrylamides bearing additional solubilizing functions. *J Med Chem* **43**(7), 1380–1397.
- Li D, Ambrogio L, Shimamura T, Kubo S, Takahashi M, Chirieac LR, Padera RF, Shapiro GI, Baum A, Himmelsbach F, et al. (2008). BIBW2992, an irreversible EGFR/HER2 inhibitor highly effective in preclinical lung cancer models. *Oncogene* **27**(34), 4702–4711.
- Wissner A, Overbeek E, Reich MF, Floyd MB, Johnson BD, Mamuya N, Rosford EC, Discifani C, Davis R, Shi X, et al. (2003). Synthesis and structure-activity relationships of 6,7-disubstituted 4-anilinoquinoline-3-carbonitriles. *J Med Chem* **46**(1), 49–63.
- Gonzales AJ, Hook KE, Althaus IW, Ellis PA, Trachet E, Delaney AM, Harvey PJ, Ellis TA, Amato DM, Nelson JM, et al. (2008). Antitumor activity and pharmacokinetic properties of PF-00299804, a second-generation irreversible pan-erbB receptor tyrosine kinase inhibitor. *Mol Cancer Ther* **7**(7), 1880–1889.
- Wang Z, Li Y, Kong D, Banerjee S, Ahmad A, Azmi AS, Ali S, Abbruzzese JL, Gallick GE, and Sarkar FH (2009). Acquisition of epithelial-mesenchymal transition phenotype of gemcitabine-resistant pancreatic cancer cells is linked with activation of the notch signaling pathway. *Cancer Res* **69**(6), 2400–2407.
- Kajiyama H, Shibata K, Terauchi M, Yamashita M, Ino K, Nawa A, and Kikkawa F (2007). Chemoresistance to paclitaxel induces epithelial-mesenchymal transition and enhances metastatic potential for epithelial ovarian carcinoma cells. *Int J Oncol* **31**(2), 277–283.
- Rho JK, Choi YJ, Lee JK, Ryoo B-Y, Na II, Yang SH, Kim CH, and Lee JC (2009). Epithelial to mesenchymal transition derived from repeated exposure to gefitinib determines the sensitivity to EGFR inhibitors in A549, a non-small cell lung cancer cell line. *Lung Cancer* **63**(2), 219–226.
- Jung M-J, Rho J-K, Kim Y-M, Jung JE, Jin YB, Ko Y-G, Lee J-S, Lee S-J, Lee JC, and Park M-J (2012). Upregulation of CXCR4 is functionally crucial for maintenance of stemness in drug-resistant non-small cell lung cancer cells. *Oncogene*. DOI: 10.1038/onc.2012.37, Epub ahead of print.

- [22] Carmi C, Galvani E, Vacondio F, Rivara S, Lodola A, Russo S, Aiello S, Bordi F, Costantino G, Cavazzoni A, et al. (2012). Irreversible inhibition of epidermal growth factor receptor activity by 3-aminopropanamides. *J Med Chem* **55**(5), 2251–2264.
- [23] Skehan P, Storeng R, Scudiero D, Monks A, McMahon J, Vistica D, Warren JT, Bokesch H, Kenney S, and Boyd MR (1990). New colorimetric cytotoxicity assay for anticancer-drug screening. *J Natl Cancer Inst* **82**(13), 1107–1112.
- [24] Giovannetti E, Zucali PA, Peters GJ, Cortesi F, D'Incecco A, Smit EF, Falcone A, Burgers JA, Santoro A, Danesi R, et al. (2010). Association of polymorphisms in AKT1 and EGFR with clinical outcome and toxicity in non-small cell lung cancer patients treated with gefitinib. *Mol Cancer Ther* **9**(3), 581–593.
- [25] Giovannetti E, Zucali PA, Assaraf YG, Leon LG, Smid K, Alecci C, Giancola F, Destro A, Gianoncelli L, Lorenzi E, et al. (2011). Preclinical emergence of vandetanib as a potent antitumour agent in mesothelioma: molecular mechanisms underlying its synergistic interaction with pemetrexed and carboplatin. *Br J Cancer* **105**(10), 1542–1553.
- [26] Alfieri RR, Galetti M, Tramonti S, Andreoli R, Mozzoni P, Cavazzoni A, Bonelli M, Fumarola C, La Monica S, Galvani E, et al. (2011). Metabolism of the EGFR tyrosin kinase inhibitor gefitinib by cytochrome P450 1A1 enzyme in EGFR-wild type non small cell lung cancer cell lines. *Mol Cancer* **10**, 143.
- [27] Giovannetti E, Labots M, Dekker H, Galvani E, Lind JSW, Sciarrillo R, Honeywell R, Smit EF, Verheul HM, and Peters GJ (2013). Molecular mechanisms and modulation of key pathways underlying the synergistic interaction of sorafenib with erlotinib in non-small-cell-lung cancer (NSCLC) cells. *Curr Pharm Des* **19**(5), 927–939.
- [28] Avan A, Crea F, Paolicchi E, Funel N, Galvani E, Marquez VE, Honeywell RJ, Danesi R, Peters GJ, and Giovannetti E (2012). Molecular mechanisms involved in the synergistic interaction of the EZH2 inhibitor 3-deazaneplanocin A with gemcitabine in pancreatic cancer cells. *Mol Cancer Ther* **11**(8), 1735–1746.
- [29] Funel N, Vasile E, Del Chiaro M, Boggi U, Falcone A, Campani D, Scarpa A, and Giovannetti E (2011). Correlation of basal EGFR expression with pancreatic cancer grading but not with clinical outcome after gemcitabine-based treatment. *Ann Oncol* **22**(2), 482–484.
- [30] Moore MJ, Goldstein D, Hamm J, Figer A, Hecht JR, Gallinger S, Au HJ, Murawa P, Walde D, Wolff RA, et al. (2007). Erlotinib plus gemcitabine compared with gemcitabine alone in patients with advanced pancreatic cancer: a phase III trial of the National Cancer Institute of Canada Clinical Trials Group. *J Clin Oncol* **25**(15), 1960–1966.
- [31] Voulgari A and Pintzas A (2009). Epithelial-mesenchymal transition in cancer metastasis: mechanisms, markers and strategies to overcome drug resistance in the clinic. *Biochim Biophys Acta* **1796**(2), 75–90.
- [32] Wheelock MJ, Shintani Y, Maeda M, Fukumoto Y, and Johnson KR (2008). Cadherin switching. *J Cell Sci* **121**(pt 6), 727–735.
- [33] Dasari V, Gallup M, Lemjabbar H, Maltseva I, and McNamara N (2006). Epithelial-mesenchymal transition in lung cancer: is tobacco the “smoking gun”? *Am J Respir Cell Mol Biol* **35**(1), 3–9.
- [34] Chen Y-T, Gallup M, Nikulina K, Lazarev S, Zlock L, Finkbeiner W, and McNamara N (2010). Cigarette smoke induces epidermal growth factor receptor-dependent redistribution of apical MUC1 and junctional β -catenin in polarized human airway epithelial cells. *Am J Pathol* **177**(3), 1255–1264.
- [35] Padrón JM, van der Wilt CL, Smid K, Smitskamp-Wilms E, Backus HH, Pizao PE, Giaccone G, and Peters GJ (2000). The multilayered postconfluent cell culture as a model for drug screening. *Crit Rev Oncol Hematol* **36**(2–3), 141–157.
- [36] Reya T, Morrison SJ, Clarke MF, and Weissman IL (2001). Stem cells, cancer, and cancer stem cells. *Nature* **414**(6859), 105–111.
- [37] Eramo A, Haas TL, and De Maria R (2010). Lung cancer stem cells: tools and targets to fight lung cancer. *Oncogene* **29**(33), 4625–4635.
- [38] Bertolini G, Roz L, Perego P, Tortoreto M, Fontanella E, Gatti L, Pratesi G, Fabbri A, Andriani F, Tinelli S, et al. (2009). Highly tumorigenic lung cancer CD133⁺ cells display stem-like features and are spared by cisplatin treatment. *Proc Natl Acad Sci USA* **106**(38), 16281–16286.
- [39] Lynch TJ, Bell DW, Sordella R, Gurubhagavatula S, Okimoto RA, Brannigan BW, Harris PL, Haserlat SM, Supko JG, Haluska FG, et al. (2004). Activating mutations in the epidermal growth factor receptor underlying responsiveness of non-small-cell lung cancer to gefitinib. *N Engl J Med* **350**(21), 2129–2139.
- [40] Miksad RA, Schnipper L, and Goldstein M (2007). Does a statistically significant survival benefit of erlotinib plus gemcitabine for advanced pancreatic cancer translate into clinical significance and value? *J Clin Oncol* **25**(28), 4506–4507. author reply 4508.
- [41] Conroy T, Desseigne F, Ychou M, Bouché O, Guimbaud R, Bécouarn Y, Adenis A, Raoul J-L, Gourgou-Bourgade S, de la Fouchardière C, et al. (2011). FOLFIRINOX versus gemcitabine for metastatic pancreatic cancer. *N Engl J Med* **364**(19), 1817–1825.
- [42] Piersma SR, Labots M, Verheul HMW, and Jiménez CR (2010). Strategies for kinome profiling in cancer and potential clinical applications: chemical proteomics and array-based methods. *Anal Bioanal Chem* **397**(8), 3163–3171.
- [43] Uzawa K, Ishigami T, Fushimi K, Kawata T, Shinozuka K, Kasamatsu A, Sakamoto Y, Ogawa K, Shiiba M, Bukawa H, et al. (2011). Targeting fibroblast growth factor receptor 3 enhances radiosensitivity in human squamous cancer cells. *Oncogene* **30**(43), 4447–4452.
- [44] Nakamoto M and Bergemann AD (2002). Diverse roles for the Eph family of receptor tyrosine kinases in carcinogenesis. *Microsc Res Tech* **59**(1), 58–67.
- [45] Infusino GA and Jacobson JR (2012). Endothelial FAK as a therapeutic target in disease. *Microvasc Res* **83**(1), 89–96.
- [46] Forest V, Campos L, Vergnon J-M, Cornillon J, and Guyotat D (2005). Characterization of the focal adhesion complex in human non-small cell lung cancer cell lines. *Anticancer Res* **25**(6B), 4135–4139.
- [47] Xiao D and He J (2010). Epithelial mesenchymal transition and lung cancer. *J Thorac Dis* **2**(3), 154–159.
- [48] Fonseca FLA, Azzalis LA, Feder D, Nogoceke E, Junqueira VBC, Valenti VE, and de Abreu LC (2011). Adhesion molecules affected by treatment of lung cancer cells with epidermal growth factor. *Lung* **189**(5), 383–389.
- [49] Thomson S, Buck E, Petti F, Griffin G, Brown E, Ramnarine N, Iwata KK, Gibson N, and Haley JD (2005). Epithelial to mesenchymal transition is a determinant of sensitivity of non-small-cell lung carcinoma cell lines and xenografts to epidermal growth factor receptor inhibition. *Cancer Res* **65**(20), 9455–9462.
- [50] Tirino V, Camerlingo R, Franco R, Malanga D, La Rocca A, Viglietto G, Rocco G, and Pirozzi G (2009). The role of CD133 in the identification and characterization of tumour-initiating cells in non-small-cell lung cancer. *Eur J Cardiothorac Surg* **36**(3), 446–453.

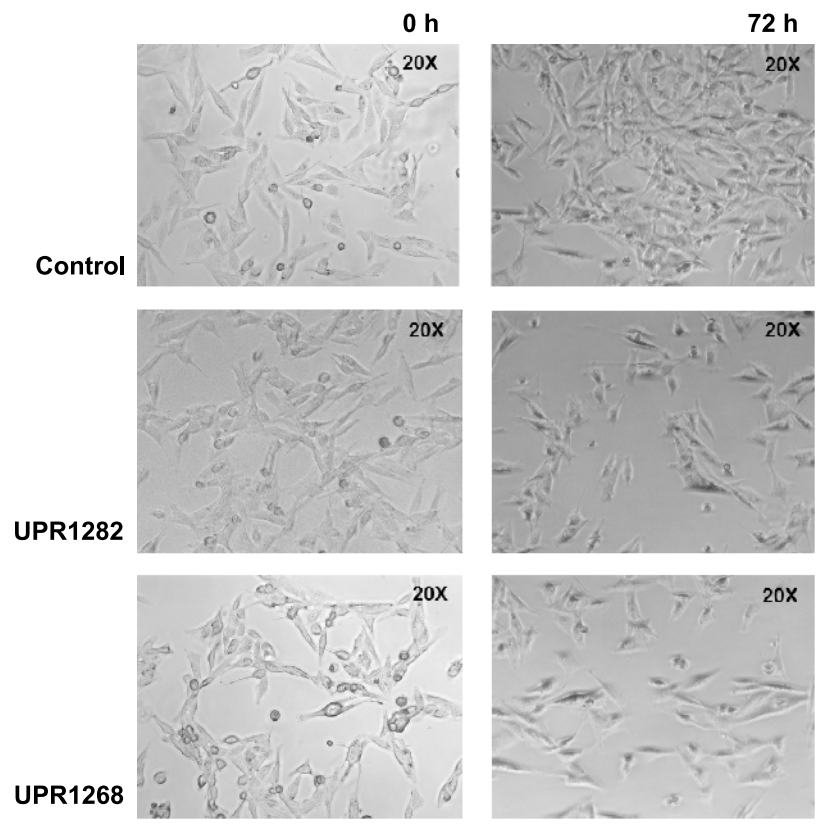


Figure W1. Cell growth inhibition. Microscopic view of the inhibitory effect of UPR1282 and UPR1268 on H1975 cell proliferation. Images were taken after 0- and 72-hour treatment with 0.1% DMSO or UPR1282 and UPR1268 at their respective IC_{50} s.